

# Topology-optimization of Structures Based on the MLPG Mixed Collocation Method

Shu Li<sup>1</sup> and S. N. Atluri<sup>2</sup>

**Abstract:** The Meshless Local Petrov-Galerkin (MLPG) “mixed collocation” method is applied to the problem of topology-optimization of elastic structures. In this paper, the topic of compliance minimization of elastic structures is pursued, and nodal design variables which represent nodal volume fractions at discretized nodes are adopted. A so-called nodal sensitivity filter is employed, to prevent the phenomenon of checkerboarding in numerical solutions to the topology-optimization problems. The example results presented in the paper demonstrate the suitability and versatility of the MLPG “mixed collocation” method, in implementing structural topology-optimization.

**Keyword:** topology optimization, meshless method, MLPG, collocation, mixed method

## 1 Introduction

The quantity of engineering literature on the topology-optimization has grown very rapidly in the last two decades, starting with the so-called homogenization method for structural topology [Bendsøe and Kikuchi (1988)]. The topology optimization problem is usually described as a material distribution design problem, a so-called 0-1 problem in nature. By optimizing an objective function, subject to constraints on the design domain, one can employ topology-optimization techniques to engineer load-bearing structures with high strength, light weight and high fracture resistance [Chiandussi, Gaviglio and Ibba (2004), Hansen and Horst(2008)]. Topology optimization has been identified as one of the most challenging and potentially useful techniques in the field of

structural design. Most research work on topology optimization for continuum structures concerns new topology models, solutions of ill-posed problems, Optimality Criteria, etc. The earlier developments in the field of topology-optimization were described in an overview paper [Eschenauer and Olhoff(2001)], and in a monograph [Bendsøe and Sigmund (2003)]. Recently, with the increase of interest in this field, various models and methods for structural topology optimization were explored, with goals of improving the computational efficiency, and alleviating numerical instabilities [Norato, Bendsøe, Haber and Tortorelli (2007), Vemaganti and Lawrence (2005), Csilino(2006), Wang and Wang (2006b,c), Wang, Lim, Khoo and Wang (2007a, b, c, 2008), Zhou and Wang (2006)].

In practice, discretization and the use of numerical methods are unavoidable in order to design a complex and practical structure. Typically, approaches for solving topology optimization problems have been mostly based on the traditional element-based methods. Almost all of the approaches presented in prior literature employ finite element methods to discretize the topological domain. An exhaustive list of publications on subject of the topology and shape optimization of structures, using the finite element and boundary element techniques, is given in [Macklerle (2003)]. However, the use of finite element methods within the optimization procedures often leads to numerical instabilities, such as mesh-dependencies, etc [Sigmund and Petersson (1998)]. It is well known that topology optimization is a far more time-consuming task, because of its complicated evolutionary procedure and refinement of mesh density.

In recent years, substantial efforts have been made in the development of the meshless meth-

<sup>1</sup> Department of Aircraft Engineering, Beijing University of Aeronautics and Astronautics, Beijing 100083, P.R. China

<sup>2</sup> Center for Aerospace Research & Education, University of California, Irvine, USA

ods, especially the MLPG method [Atluri and Zhu(1998), Atluri and Shen(2002a, 2002b), and Atluri(2004)]. These meshless methods have inherent advantages over the element-based approaches, due to the elimination of the mesh, and the ease with which a high-order continuity of the trial functions is achieved. Atluri, Liu, and Han (2006) have recently proposed a very attractive and promising method which they call the MLPG “mixed collocation” method. In this method, a very simple formulation is achieved, and the computer implementation is very convenient. These benefits are realized, without any numerical integration either over a local domain or over the local boundary. This method improves the computational efficiency and the ease of implementation of the meshless method, especially for topology-optimization.

The present paper is dedicated to topology-optimization of continuum structures using the MLPG “mixed collocation” method. The main features of this paper are: the use of the MLPG “mixed collocation” method to discretize the design domain, and the choice of nodal volume fractions as the optimization design variables, instead of the element volume fractions. We employ the widely used density-like function called SIMP (Solid Isotropic Material with Penalization) model for the penalization. The objective of topology-optimization is to minimize the compliance for an optimal layout of structures, under a given set of loads and boundary conditions. The method of Optimality Criteria (OC) is employed to solve the topology optimization problem. Here, structural volume fractions become a function of the nodal volume fractions. Compared with the element-based methods such as in [Guest, Prévost and Belytschko (2004)], these nodal values need not be interpolated or projected onto the element, in order to obtain the familiar element-wise volume fractions which can determine the topology of structures. The numerical examples presented here demonstrate that the MLPG mixed collocation method renders the solution of the optimization problem to be highly accurate and computationally efficient.

The framework of this paper is as follows: Section

2 briefly reviews the major aspects of the MLPG mixed collocation method. Section 3 gives a formulation for the structural topology optimization, a heuristic scheme of the optimality criteria (OC) method, and the filtering principle. Section 4 presents some examples. Finally, we present some conclusions in Section 5.

## 2 MLPG Mixed Collocation Method

### 2.1 The moving least squares (MLS)

The moving least squares (MLS) approximation is often chosen as the interpolation function in a meshless approximation of the trial function. The MLPG Mixed Collocation Method adopts the MLS interpolation to approximate a function  $\mathbf{u}(\mathbf{x})$  over a number of nodes randomly spread within the domain of influence. The approximated function  $\mathbf{u}(\mathbf{x})$  can be written as [Atluri (2004)]

$$\mathbf{u}(\mathbf{x}) = \mathbf{p}^T(\mathbf{x})\mathbf{a}(\mathbf{x}) \quad (1)$$

where  $\mathbf{p}^T(\mathbf{x})$  is a monomial basis which can be expressed as  $\mathbf{p}^T(\mathbf{x}) = [1, x_1, x_2]$  for two-dimensional problems and  $\mathbf{p}^T(\mathbf{x}) = [1, x_1, x_2, x_3]$  for three dimensional problems, respectively.  $\mathbf{a}(\mathbf{x})$  is a vector of undetermined coefficients, which can be obtained by minimizing the weighted discrete  $L_2$  norm, defined as

$$J(\mathbf{x}) = \sum_{I=1}^m \mathbf{w}_I(\mathbf{x}) [\mathbf{p}^T(\mathbf{x}_I)\mathbf{a}(\mathbf{x}) - \hat{u}^I]^2 \quad (2)$$

where  $\{\mathbf{x}_I\}, (I = 1, 2, \dots, m)$  are scattered local points (nodes) to approximate the function  $\mathbf{u}(\mathbf{x})$ ,  $\mathbf{w}_I$  are the weight functions and  $\hat{u}^I$  are the fictitious nodal values. After the coefficient vector  $\mathbf{a}(\mathbf{x})$  is obtained, we substitute it into Eq. (1). The function  $\mathbf{u}(\mathbf{x})$  can be approximated by these fictitious nodal values, as

$$u(\mathbf{x}) = \sum_{I=1}^m \Psi^I(\mathbf{x}) \hat{u}^I \quad (3)$$

where  $\hat{u}^I$  is the virtual nodal value at node  $I$ , and  $\Psi^I(\mathbf{x})$  is the shape function. The detailed formulations and discussions for the MLS interpolation, using the true nodal values can be found in Atluri (2004).

Generally speaking, the MLS shape function does not have the Dirac Delta property, namely

$$u^I \equiv u(\mathbf{x}^I) = \sum_{J=1}^m \Psi^J(\mathbf{x}) \hat{u}^I \neq \hat{u}^I \quad (4)$$

However, with the mapping relationship between the virtual and true nodal values [Eq. (4)], it is straightforward to establish the trial functions in the true nodal-values space as

$$u(\mathbf{x}) = \sum_{I=1}^m \Phi^I(\mathbf{x}) u^I \quad (5)$$

## 2.2 Equilibrium equations

We consider a linear elastic body  $\Omega$  undergoing infinitesimal deformations. The equilibrium equation can be expressed as

$$\nabla \cdot \boldsymbol{\sigma} + \mathbf{f} = \mathbf{0} \quad (6)$$

subject to the boundary conditions:

$$\begin{aligned} \mathbf{u} &= \bar{\mathbf{u}} \quad \text{on } \Gamma_u \\ \mathbf{t} &= \bar{\mathbf{t}} \quad \text{on } \Gamma_t \end{aligned} \quad (7)$$

In which  $\boldsymbol{\sigma}$  is the stress tensor,  $\nabla$  is the gradient vector,  $\mathbf{f}$  is the body force vector;  $\mathbf{u}$  is the displacement vector,  $\mathbf{t}$  is the traction vector, and  $\mathbf{n}$  is the outward unit normal to the boundary  $\Gamma$ .

Within the general MLPG framework [Atluri(2004)], one may choose the Dirac Delta function as the test function for the unsymmetric local weak form, and apply it to each nodal point. The momentum balance equation is enforced at the nodal points, as

$$[\nabla \cdot \boldsymbol{\sigma}](\mathbf{x}^I) + \mathbf{f}(\mathbf{x}^I) = \mathbf{0} \quad (8)$$

where  $\{\mathbf{x}^I\}$ , ( $I = 1, 2, \dots, N$ ) are the distributed nodes, and  $N$  is the number of total distributed nodes in the solution domain. In the present mixed scheme, we interpolate the displacement vector  $\mathbf{u}(\mathbf{x})$  and the stress tensor  $\boldsymbol{\sigma}(\mathbf{x})$  independently, using the same shape functions obtained from the MLS approximation [Eq. (3)], namely

$$\mathbf{u}(\mathbf{x}) = \sum_{J=1}^m \Phi^J(\mathbf{x}) \mathbf{u}^J \quad (9)$$

$$\boldsymbol{\sigma}(\mathbf{x}) = \sum_{J=1}^m \Phi^J(\mathbf{x}) \boldsymbol{\sigma}^J \quad (10)$$

Here,  $\mathbf{u}^J$  and  $\boldsymbol{\sigma}^J$  are the nodal displacement vector and stress vector [note that the stress tensor is now symbolically re-written as a stress-vector] at node  $J$ , respectively. In the case of the isotropic linear elastic problem, the relation between the stress vector  $\boldsymbol{\sigma}$  and the strain vector  $\boldsymbol{\varepsilon}$  can be written as

$$\boldsymbol{\sigma} = \mathbf{D} \cdot \boldsymbol{\varepsilon} \quad (11)$$

$$\boldsymbol{\varepsilon} = \mathbf{L}^* \cdot \mathbf{u} \quad (12)$$

where,  $\mathbf{L}^*$  a differential operator, for the present 2D problem,

$$\mathbf{D} = \frac{E}{1-\nu^2} \begin{bmatrix} 1 & \nu & 0 \\ \nu & 1 & 0 \\ 0 & 0 & \frac{1-\nu}{2} \end{bmatrix}$$

with  $E$  the Young's modulus,  $\nu$  the Poisson's ratio. Upon substituting the stress interpolation Eq. (10) into Eq. (8), we have

$$\begin{aligned} \sum_{J=1}^m \nabla \cdot \Phi^J(\mathbf{x}^I) \cdot \boldsymbol{\sigma}^J + \mathbf{f}(\mathbf{x}^I) &= \mathbf{0}; \\ \text{for } \mathbf{I} &= 1, 2, \dots, N \end{aligned} \quad (13)$$

It clearly shows that there are no second derivatives of the shape functions for the displacements involved in the system equations, due to the independent interpolation of the stress variables. It is well known that in the meshless approximation, specifically the MLS, usually results in a very complex form of the second derivatives. The Eq. (13) has less number of equations than the number of the independent stress variables, because the nodal stress variables are more than the displacement ones. Therefore, we need to establish some more equations in addition to Eq. (11) through the stress displacement relation. The standard collocation method may be applied to enforce the stress displacement relation at each nodal point. For linear elasticity problems, this relation can be written as

$$\boldsymbol{\sigma}(\mathbf{x}^I) = \mathbf{D} \cdot \boldsymbol{\varepsilon}(\mathbf{x}^I) = \mathbf{D} \cdot \mathbf{L}^* \cdot \mathbf{u}(\mathbf{x}^I) \quad (14)$$

After substituting the displacement interpolation Eq. (9) into Eq. (14), we have

$$\boldsymbol{\sigma}^J = \sum_{J=1}^m \mathbf{DB}^J(\mathbf{x}^I) \mathbf{u}^I \quad (15)$$

where

$$\mathbf{B}^J(\mathbf{x}^I) = \begin{bmatrix} \Phi_{,x}^J(\mathbf{x}^I) & 0 \\ 0 & \Phi_{,y}^J(\mathbf{x}^I) \\ \Phi_{,y}^J(\mathbf{x}^I) & \Phi_{,x}^J(\mathbf{x}^I) \end{bmatrix} \quad (16)$$

$$\boldsymbol{\sigma}^J = [\sigma_x^J \quad \sigma_y^J \quad \tau_{xy}^J]^T$$

$$\mathbf{u}^J = [u_x^J \quad u_y^J]^T$$

Eq. (13) and Eq. (14) can be rewritten in the form as follows, respectively:

$$\mathbf{K}_S \cdot \boldsymbol{\sigma} = \mathbf{f}_b \quad (17)$$

$$\boldsymbol{\sigma} = \mathbf{T} \cdot \mathbf{u} \quad (18)$$

In which  $\mathbf{f}_b$  is the body force vector.

We set  $\mathbf{B}_{IJ} = \mathbf{B}^J(\mathbf{x}^I)$ , thus

$$\mathbf{K}_S = \begin{bmatrix} \mathbf{B}_{11}^T & \mathbf{B}_{12}^T & \cdots & \mathbf{B}_{1n}^T \\ \mathbf{B}_{21}^T & \mathbf{B}_{22}^T & \cdots & \mathbf{B}_{2n}^T \\ \vdots & \vdots & \vdots & \vdots \\ \mathbf{B}_{n1}^T & \mathbf{B}_{n1}^T & \cdots & \mathbf{B}_{nn}^T \end{bmatrix}$$

$$\mathbf{T} = \mathbf{D} \cdot \begin{bmatrix} \mathbf{B}_{11} & \mathbf{B}_{12} & \cdots & \mathbf{B}_{1n} \\ \mathbf{B}_{21} & \mathbf{B}_{22} & \cdots & \mathbf{B}_{2n} \\ \vdots & \vdots & \vdots & \vdots \\ \mathbf{B}_{n1} & \mathbf{B}_{n1} & \cdots & \mathbf{B}_{nn} \end{bmatrix}$$

and

$$\boldsymbol{\sigma} = \begin{bmatrix} \boldsymbol{\sigma}^1 \\ \boldsymbol{\sigma}^2 \\ \vdots \\ \boldsymbol{\sigma}^J \\ \vdots \\ \boldsymbol{\sigma}^N \end{bmatrix}, \quad \mathbf{u} = \begin{bmatrix} \mathbf{u}^1 \\ \mathbf{u}^2 \\ \vdots \\ \mathbf{u}^J \\ \vdots \\ \mathbf{u}^N \end{bmatrix}$$

Let

$$\bar{\mathbf{K}} = \mathbf{K}_S \cdot \mathbf{T} \quad (19)$$

which yields the well known formulation of equilibrium equation

$$\bar{\mathbf{K}} \mathbf{u} = \mathbf{f}_b \quad (20)$$

where

$$\bar{\mathbf{K}}_{IJ} = \sum_{K=1}^m \mathbf{B}_{IK}^T \mathbf{DB}_{KJ} \quad (21)$$

### 2.3 Boundary Conditions

The traction boundary conditions are enforced at each of the traction boundary nodes  $K$ , as:

$$\mathbf{n}^K \cdot \boldsymbol{\sigma}^K = \bar{\mathbf{t}}^K, \quad \text{for } K = 1, \dots, S \quad (22)$$

where  $S$  is the number of total traction boundary nodes, the matrix  $\mathbf{n}^K$  is the transformation matrix between the coordinates, as

$$\mathbf{n}^K = \begin{bmatrix} n_x^K & 0 & n_y^K \\ 0 & n_y^K & n_x^K \end{bmatrix}$$

and

$$\boldsymbol{\sigma}^K = [\sigma_x^K \quad \sigma_y^K \quad \tau_{xy}^K]^T, \quad \bar{\mathbf{t}}^K = [\bar{t}_x^K \quad \bar{t}_y^K]^T$$

Assuming  $\boldsymbol{\sigma}_1$  and  $\boldsymbol{\sigma}_2$  represent the known and unknown stress vectors, respectively. Hence Eq.(20) can be written as

$$\bar{\mathbf{K}}_1 \cdot \boldsymbol{\sigma}_1 + \bar{\mathbf{K}}_2 \cdot \boldsymbol{\sigma}_2 = \mathbf{f}_b \quad (23)$$

where

$$\boldsymbol{\sigma}_1 = \mathbf{T}_1 \cdot \mathbf{u} \quad (24)$$

$$\boldsymbol{\sigma}_2 = \mathbf{T}_2 \cdot \mathbf{u} \quad (25)$$

Premultiplying Eq. (22) by the penalty number  $\alpha$  and the transpose of the transformation matrix  $\mathbf{n}$ , we obtain:

$$\alpha \mathbf{n}^T \cdot \mathbf{n} \cdot \boldsymbol{\sigma}_1 = \alpha \mathbf{n}^T \cdot \bar{\mathbf{t}} \quad (26)$$

where

$$\mathbf{n} = \begin{bmatrix} \mathbf{n}^1 & & & & 0 \\ & \mathbf{n}^2 & & & \\ & & \ddots & & \\ & & & \mathbf{n}^K & \\ & & & & \ddots \\ 0 & & & & & \mathbf{n}^S \end{bmatrix},$$

$$\boldsymbol{\sigma}_1 = \begin{bmatrix} \boldsymbol{\sigma}^1 \\ \boldsymbol{\sigma}^2 \\ \vdots \\ \boldsymbol{\sigma}^K \\ \vdots \\ \boldsymbol{\sigma}^S \end{bmatrix}, \quad \bar{\mathbf{t}} = \begin{bmatrix} \bar{\mathbf{t}}^1 \\ \bar{\mathbf{t}}^2 \\ \vdots \\ \bar{\mathbf{t}}^K \\ \vdots \\ \bar{\mathbf{t}}^S \end{bmatrix}$$

It is easy to obtain

$$\boldsymbol{\sigma}_1 + \alpha \mathbf{n}^T \cdot \mathbf{n} \cdot \boldsymbol{\sigma}_1 = \mathbf{T}_1 \cdot \mathbf{u} + \alpha \mathbf{n}^T \cdot \bar{\mathbf{t}} \quad (27)$$

and

$$\boldsymbol{\sigma}_1 = (\mathbf{I} + \alpha \mathbf{n}^T \cdot \mathbf{n})^{-1} (\mathbf{T}_1 \cdot \mathbf{u} + \alpha \mathbf{n}^T \cdot \bar{\mathbf{t}}) \quad (28)$$

where I is unit matrix.

Let

$$\mathbf{Q} = (\mathbf{I} + \alpha \mathbf{n}^T \cdot \mathbf{n})^{-1} \quad (29)$$

then

$$\boldsymbol{\sigma}_1 = \mathbf{Q} \cdot \mathbf{T}_1 \cdot \mathbf{u} + \alpha \mathbf{Q} \cdot \mathbf{n}^T \cdot \bar{\mathbf{t}} \quad (30)$$

By substituting Eq. (30) into Eq.(23), we can obtain a discretized system which is expressed as

$$\mathbf{K} \cdot \mathbf{u} = \mathbf{f} \quad (31)$$

where

$$\begin{aligned} \mathbf{K} &= \bar{\mathbf{K}}_1 \cdot \mathbf{Q} \cdot \mathbf{T}_1 + \bar{\mathbf{K}}_2 \cdot \mathbf{T}_2 \\ \mathbf{f} &= \mathbf{f}_b - \alpha \bar{\mathbf{K}}_1 \cdot \mathbf{Q} \cdot \mathbf{n}^T \cdot \bar{\mathbf{t}} \end{aligned} \quad (32)$$

### 3 Topology optimization problem

#### 3.1 Problem formulation

Topology-optimization implies the optimal distribution of material in a structure, so as to minimize its compliance, subject to the specified constraints of the total material to be used. Here,

‘compliance’ is defined as the product of the external loads and the corresponding displacements. According to Eq.(31), the mean compliance of a structure is formulated as follows:

$$C = \mathbf{f}^T \cdot \mathbf{u} \quad (33)$$

where  $\mathbf{u}$  is the global displacement vector,  $\mathbf{f}$  is the force vector. Also, the above expression can also be written, for linear response, as:

$$C = \mathbf{u}^T \mathbf{K} \mathbf{u} \quad (34)$$

In practice, Eq.(34) is discretized using the MLPG Mixed Collocation Method. The design domain  $\Omega$  (Fig.1) is partitioned into  $N$  nodes. For an arbitrary node  $i$ , if the number of nodes around point  $i$  which influence the trial function at node  $i$  is  $r$ , a sub-system consists of these  $r$  nodes. In this sub-system, we have

$$\mathbf{k}_i \mathbf{u}_i = \mathbf{f}_i \quad (35)$$

where  $\mathbf{u}_i$  is the displacement vector and  $\mathbf{k}_i$  is the ‘‘stiffness’’ matrix constructed in the same way as Eq.(19). The discretized formulation of Eq.(34) becomes

$$C = \sum_{i=1}^N \mathbf{u}_i^T \mathbf{k}_i \mathbf{u}_i \quad (36)$$

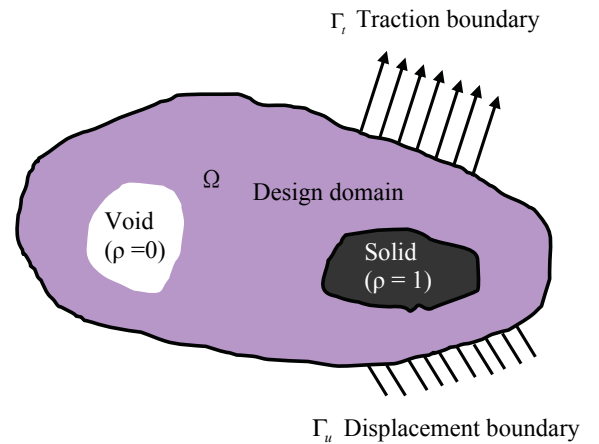


Figure 1: Two-dimensional design domain for topology optimization

If we consider the nodal volume fractions  $\rho_i$  as the design variables, then the topology optimization

problem for minimizing the compliance can thus be stated, with the volume constraint  $V^*$  as follows:

$$\begin{aligned} \min_{\boldsymbol{\rho}} \quad & C(\boldsymbol{\rho}) = \mathbf{u}^T \mathbf{K} \mathbf{u} = \sum_{i=1}^N \mathbf{u}_i^T \mathbf{k}_i \mathbf{u}_i \\ \text{subject to} \quad & V(\boldsymbol{\rho}) = \sum_{i=1}^N \rho_i V_i = V^* \\ & \mathbf{K} \mathbf{u} = \mathbf{f} \\ & 0 < \rho_{\min} \leq \rho_i \leq 1 \end{aligned} \quad (37)$$

where  $\boldsymbol{\rho}$  is the vector consisted of design variable  $\rho_i$ ,  $\rho_{\min}$  is the minimum allowable relative volume fractions (non-zero to avoid singularity),  $N$  is the number of nodes to discretize the design domain, and  $V^*$  is the prescribed volume.  $V(\boldsymbol{\rho})$  is the total volume of material.

Setting  $\rho_{\min}$  to a positive value keeps the “stiffness” matrix  $\mathbf{k}_i$  from becoming singular. The artificial variable  $\rho_i$  is considered as an indicator of the local material volume  $V_i$ . The final material volume  $V^*$  is linearly related to the design variables.

To avoid intermediate volume fraction values  $\rho_i$  (between 0 and 1), a SIMP-like model (Solid Isotropic Microstructure with Penalty) is adopted in the proposed topology optimization method. In this SIMP-like model, the penalized “stiffness” matrix  $\mathbf{k}_i$  is given by

$$\mathbf{k}_i = (\rho_i)^p \mathbf{k}_i^0 \quad (38)$$

$\mathbf{k}_i^0$  is the initial value of the matrix  $\mathbf{k}_i$ ,  $p$  is the penalization power (typically  $p = 3$ ). Fig.2 displays the relative “stiffness” ratio vs. volume fraction values  $\rho_i$ , for different values of the penalization power  $p$ .

Due to the asymmetry of the matrix  $\mathbf{K}$  in the MLPG “Mixed Collocation” method, the sensitivities of the compliance respect to design variable  $\rho_i$  can be derived from the expression of Eq.(33), as follows:

$$\begin{aligned} \frac{\partial C}{\partial \rho_i} &= \mathbf{f}^T \cdot \frac{\partial \mathbf{u}}{\partial \rho_i} = (\mathbf{K} \mathbf{u})^T \frac{\partial \mathbf{u}}{\partial \rho_i} = \mathbf{u}^T \mathbf{K}^T \frac{\partial \mathbf{u}}{\partial \rho_i} \\ &= \mathbf{u}_i^T \mathbf{k}_i^T \frac{\partial \mathbf{u}_i}{\partial \rho_i} \end{aligned} \quad (39)$$

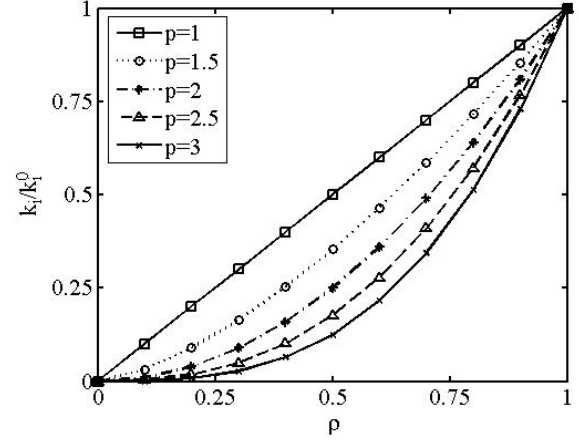


Figure 2: SIMP-like model for different values of the penalization power  $p$

We consider the discretized formulations  $\mathbf{k}_i \mathbf{u}_i = \mathbf{f}_i$  and  $C = \sum_{i=1}^N \mathbf{u}_i^T \mathbf{k}_i \mathbf{u}_i$ . Because the derivative of  $\mathbf{f}_i$  with respect to  $\rho_i$  is null, we can obtain:

$$\frac{\partial \mathbf{k}_i}{\partial \rho_i} \mathbf{u}_i = -\mathbf{k}_i \frac{\partial \mathbf{u}_i}{\partial \rho_i} \quad (40)$$

Substituting Eq.(38) into Eq.(40), we have

$$p(\rho_i)^{p-1} \mathbf{k}_i^0 \mathbf{u}_i = -(\rho_i)^p \mathbf{k}_i^0 \frac{\partial \mathbf{u}_i}{\partial \rho_i}$$

i.e.

$$\frac{\partial \mathbf{u}_i}{\partial \rho_i} = -\frac{1}{\rho_i} p \mathbf{u}_i \quad (41)$$

Finally, the expression of Eq.(39) is written as

$$\begin{aligned} \frac{\partial C}{\partial \rho_i} &= \mathbf{u}_i^T \mathbf{k}_i^T \frac{\partial \mathbf{u}_i}{\partial \rho_i} \\ &= \mathbf{u}_i^T \left( (\rho_i)^p \mathbf{k}_i^0 \right)^T \left( -\frac{1}{\rho_i} p \mathbf{u}_i \right) \\ &= -p(\rho_i)^{p-1} \mathbf{u}_i^T (\mathbf{k}_i^0)^T \mathbf{u}_i \end{aligned} \quad (42)$$

### 3.2 The optimality criteria (OC) method

The discrete topology optimization problem (39) usually has a large number of design variables. It is natural to use iterative optimization methods for such a problem. Here, we choose the popular Optimality Criteria (OC) method for iterative optimization. Optimality Criteria methods seek the

optimum in the space of the Lagrange multipliers relevant to the active constraints based upon the Kuhn-Tucker (K-T) Conditions. These K-T Conditions are an extension of the Lagrangian theory to solve the general classical single-objective non-linear programming problem. They provide powerful tools to search optimal solutions. The computational time of the OC method is highly dependent on the number of active constraints. In this paper, the optimality criteria (OC) was formulated in a form suitable for incorporation in the meshless method codes.

The Lagrangian for the optimization problem [Eq.(39)] is defined as

$$L(\boldsymbol{\rho}) = C + \lambda_1 \left( \sum_{i=1}^N \rho_i V_i - V^* \right) + \boldsymbol{\Lambda}^T (\mathbf{K}\mathbf{u} - \mathbf{f}) + \sum_{i=1}^N \mu_1^i (\rho_{\min} - \rho_i) + \sum_{i=1}^N \mu_2^i (\rho_i - 1) \quad (43)$$

where  $\lambda_1$  and  $\mu_i$  are Lagrange multipliers for the equality and inequality constraints, respectively.  $\boldsymbol{\Lambda}$  is the Lagrange multiplier vector. The necessary conditions for optimality can be obtained by using the Kuhn-Tucker conditions as follows:

$$\frac{\partial L}{\partial \rho_i} = 0, \quad i = 1, 2, \dots, N$$

Differentiating (43) with respect to  $\rho_i$  and manipulating the terms, the Kuhn-Tucker optimality condition can be written for problems [Eq.(37)] subject to multiple constraints as follows

$$\left\{ \begin{array}{l} \frac{\partial L}{\partial \rho_i} = \frac{\partial C}{\partial \rho_i} + \lambda_1 \frac{\partial V}{\partial \rho_i} + \boldsymbol{\Lambda}^T \frac{\partial (\mathbf{K}\mathbf{u})}{\partial \rho_i} - \mu_1 + \mu_2 = 0 \\ V(\boldsymbol{\rho}) = \sum_{i=1}^N \rho_i V_i - V^* = 0 \\ \quad \text{(the equality constraints)} \\ \mathbf{K}\mathbf{u} = \mathbf{f} \quad \text{(the equality constraints)} \\ \rho_{\min} - \rho_i \leq 0 \quad \text{(the inequality constraints)} \\ \rho_i - 1 \leq 0 \quad \text{(the inequality constraints)} \\ \mu_1 (\rho_{\min} - \rho_i) = 0 \\ \mu_2 (\rho_i - 1) = 0 \\ \mu_i \geq 0 \quad i = 1, 2 \end{array} \right. \quad (44)$$

Note:  $\lambda_1$  and  $\boldsymbol{\Lambda}$  are unrestricted in sign, corresponding to the equality constraints. It is clear that the efficiency of the OC method is determined mainly by the number of active constraints. If  $\rho_{\min} < \rho_i < 1$ , the lower and upper bounds of the design variables are inactive, then we have  $\mu_1 = \mu_2 = 0$ . If  $\rho_i = \rho_{\min}$ , the lower bound of the design variables are active, then we have  $\mu_1 \geq 0, \mu_2 = 0$ . If  $\rho_i = \rho_{\max}$ , the upper bound of the design variables are active, then  $\mu_1 = 0, \mu_2 \geq 0$ . and (44) yields:

$$\left\{ \begin{array}{l} \frac{\partial C}{\partial \rho_i} + \lambda_1 \frac{\partial V}{\partial \rho_i} + \boldsymbol{\Lambda}^T \frac{\partial (\mathbf{K}\mathbf{u})}{\partial \rho_i} = 0 \quad \text{if } \rho_{\min} < \rho_i < 1 \\ \frac{\partial C}{\partial \rho_i} + \lambda_1 \frac{\partial V}{\partial \rho_i} + \boldsymbol{\Lambda}^T \frac{\partial (\mathbf{K}\mathbf{u})}{\partial \rho_i} \geq 0 \quad \text{if } \rho_i = \rho_{\min} \\ \frac{\partial C}{\partial \rho_i} + \lambda_1 \frac{\partial V}{\partial \rho_i} + \boldsymbol{\Lambda}^T \frac{\partial (\mathbf{K}\mathbf{u})}{\partial \rho_i} \leq 0 \quad \text{if } \rho_i = \rho_{\max} \\ V(\boldsymbol{\rho}) = \sum_{i=1}^N \rho_i V_i - V^* = 0 \\ \quad \text{(the equality constraints)} \\ \mathbf{K}\mathbf{u} = \mathbf{f} \quad \text{(the equality constraints)} \\ \mu_i \geq 0 \quad i = 1, 2 \end{array} \right. \quad (45)$$

The above sensitivity of a node is dependent on several surrounding points. For different positions, the number of nodes around one point may differ. So the sensitivity analysis is more complex and time consuming when compared with the case of element-based methods.

To derive the iterative formulation more conveniently, only the equality cases in Eq.(45) are used in the present illustration, i.e.

$$\frac{\partial C}{\partial \rho_i} + \lambda_1 \frac{\partial V}{\partial \rho_i} + \boldsymbol{\Lambda}^T \left( \frac{\partial \mathbf{K}}{\partial \rho_i} \mathbf{u} + \mathbf{K} \frac{\partial \mathbf{u}}{\partial \rho_i} \right) = 0$$

Utilizing the expression  $\mathbf{K}\mathbf{u} = \mathbf{f}$ , it is easy to obtain

$$\frac{\partial \mathbf{K}}{\partial \rho_i} \mathbf{u} + \mathbf{K} \frac{\partial \mathbf{u}}{\partial \rho_i} = 0$$

then

$$-p(\rho_i)^{p-1} \mathbf{u}_i^T (\mathbf{k}_i^0)^T \mathbf{u}_i + \lambda_1 V_i = 0 \quad (46)$$

Set

$$B_i = \frac{p(\rho_i)^{p-1} \mathbf{u}_i^T (\mathbf{k}_i^0)^T \mathbf{u}_i}{\lambda_1 V_i} = 1 \quad (47)$$

Eq.(47) is regarded as an Optimally Criteria (OC) based on the discretization of the MLPG Mixed Collocation Method. Thus, we can update the design variables as follows:

$$\rho_i^{new} = \begin{cases} \max(\rho_{\min}, \rho_i - m) & \text{if } \rho_i B_i^\eta \leq \max(\rho_{\min}, \rho_i - m) \\ \rho_i B_i^\eta & \text{if } \max(\rho_{\min}, \rho_i - m) < \rho_i B_i^\eta \\ & < \min(1, \rho_i + m) \\ \min(1, \rho_i + m) & \text{if } \min(1, \rho_i + m) \leq \rho_i B_i^\eta \end{cases} \quad (48)$$

Where  $m$  is the limit ([Bendsøe and Kikuchi (1988)]), which represents the maximum allowable change in the relative nodal volume fractions  $\rho_i$  in the OC iteration.  $\eta$  is the damping coefficient. This updating scheme was often adopted in many presented papers. The values of  $m$  and  $\eta$  influence the convergence of the scheme, and they are chosen by experience ([Bendsøe and Kikuchi (1988)]).

The penalty parameter  $p$  is set to be 3, and the numerical damping coefficient  $\eta$  is set to 0.5. The Lagrange multiplier for the volume constraint  $\lambda_1$  is determined at each OC iteration using a bisectioning algorithm, as in the paper [Sigmund (2001)].

### 3.3 Filtering principle

Here we describe the principle of suppressing checkerboard patterns, which is a familiar problem in topology optimization when numerical stability is not guaranteed. The appearance of checkerboarding causes difficulties in interpreting and fabricating topology-optimized structural components. Sigmund (1994, 1997) developed a sensitivity filter method for preventing numerical instabilities from occurring. Filtering techniques have become quite popular in topology optimization [Wang; Lim, Khoo and Wang (2008)]. To tackle checkerboarding, a scheme similar to the filtering method is incorporated in the optimization algorithms based on the meshless discretization. In this scheme, we modify the de-

sign sensitivity of any specific node depending on a weighted average of the node sensitivities in a connected neighborhood. The principle works by modifying the nodal sensitivities as follows

$$\frac{\partial \hat{C}}{\partial \rho_i} = \frac{1}{\rho_i \sum_{f=1}^m \hat{H}_f} \sum_{f=1}^m \hat{H}_f \rho_f \frac{\partial C}{\partial \rho_f} \quad (49)$$

Here, the convolution operator (weight factor) is written as

$$\hat{H}_f = r_{\min} - \text{dist}(n, f) \\ \{f \in M \mid \text{dist}(n, f) \leq r_{\min}\}, \\ n = 1, \dots, m \quad (50)$$

and the operator  $\text{dist}(n, f)$  is defined as the distance between node  $n$  and node  $f$ . The convolution operator  $\hat{H}_f$  is zero outside the filter area, and decays linearly with the distance from node  $f$ .

## 4 Numerical examples

In this section, we present several numerical examples (cantilever and MBB-beams). They are used to illustrate the suitability of the MLPG Mixed Collocation Method for solving topology optimization problems with volume constraints. All the following examples are treated here as being dimensionless.

### 4.1 Verification of the validity and convergence

The topology-optimization problem is an ill-posed problem, with a lack of proof existence of solutions, since it often results in a complex material distribution [Eschenauer and Olhoff(2001)]. The convergence of solutions can not be guaranteed numerically. The validity and convergence are the important areas of concern for the solution of the topology optimization problem. We want to compare the results by the present method with the ones by finite element method (FEM).

#### Example 1:

The first example is that of a short cantilever beam as shown in Fig. 3. The design domain is fixed along the left edge and a concentrated vertical load  $P$  is applied at the bottom corner of the free (right) end of the beam.

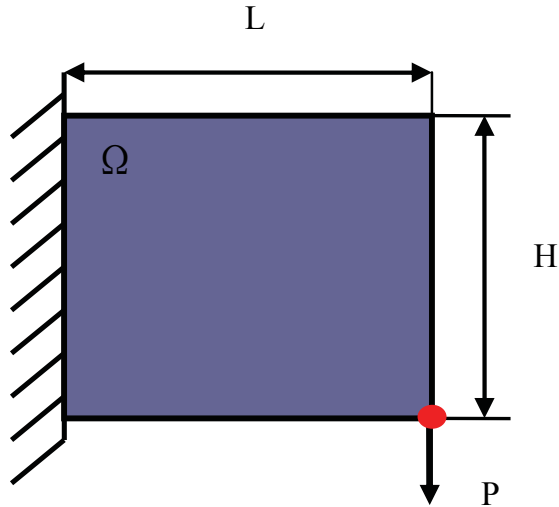


Figure 3: Cantilever beam I (L=H)

To determine an optimum structural layout, the square ‘design domain’ ( $L=H$ ) is discretized by the MLPG Mixed Collocation Method using  $20 \times 20$ ,  $40 \times 40$ ,  $80 \times 80$  uniformly distributed nodes, respectively.

The same problem is also solved by using the finite element method (FEM) by Sigmund(2001) for mesh refinements of  $20 \times 20$ ,  $40 \times 40$ ,  $80 \times 80$  elements. The optimized topology results using the meshless method and finite element method are shown in Fig. 4 and Fig.5, respectively. It can be seen that for this example, the similar topologies were obtained by two different algorithms.

**Example 2:**

The second case is the so-called MBB beam [Zhou and Rozvany 1991] which only the right half-domain (Fig.7) is used for the analysis. The design domain is discretized into  $60 \times 20$ ,  $90 \times 30$ ,  $120 \times 40$  uniformly distributed nodes in the half-domain, respectively. The left bottom is assumed to be fixed, and the right one is assumed to be on a roller. The concentrated load  $P$  is applied at the middle of the top of the beam. As a comparison, the considered problem was also investigated by using finite element method (FEM). The mesh refinements are of  $60 \times 20$ ,  $90 \times 30$ ,  $120 \times 40$  elements in the half-domain, respectively. The solutions are given in Fig.8 and Fig.9. After comparing these solutions, it can be seen from that

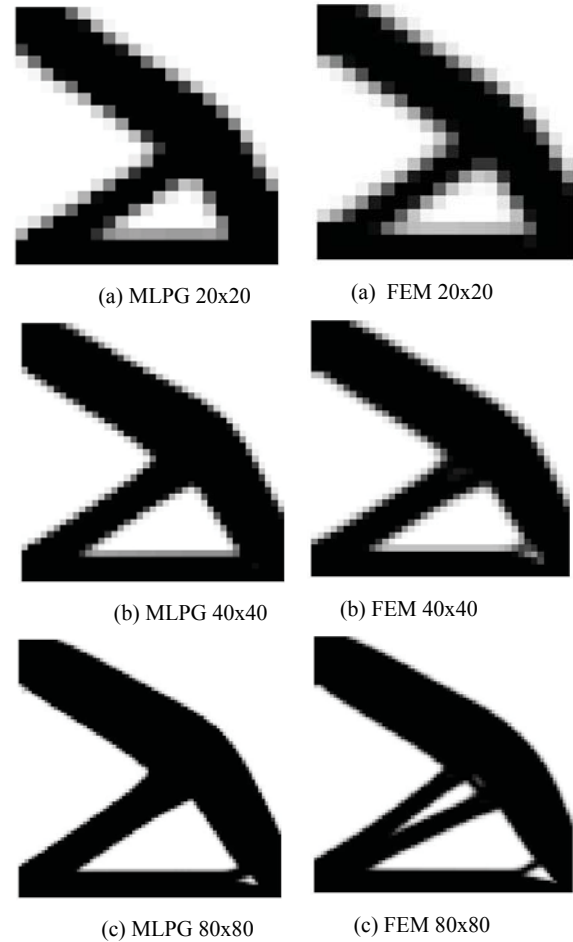


Figure 4: Topology optimization results of the cantilever beam by the MLPG Mixed Collocation Method

Figure 5: Topology optimization results of the cantilever beam by FEM methods

similar topologies can be obtained in the MLPG ‘Mixed Collocation’ method, as in the FEM.

Fig.6 and Fig.10 give three curves of convergence of the cantilever and MBB beams’ mean compliance, respectively. The almost monotonic and uniform convergence can be observed from these figures. The mean compliances steadily decrease as the iteration number is increased. Their convergence characteristics are very similar. Note that for both the above examples, the iterative performances of the discretization differ very little.

The validity and convergence of the present topology optimization method are verified by the ex-

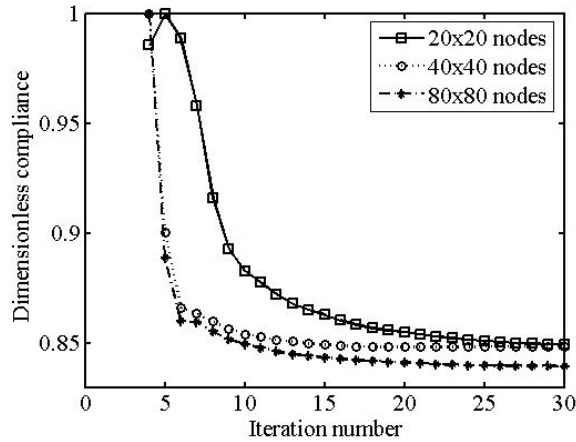


Figure 6: Convergence history of the cantilever beam compliance using the present method

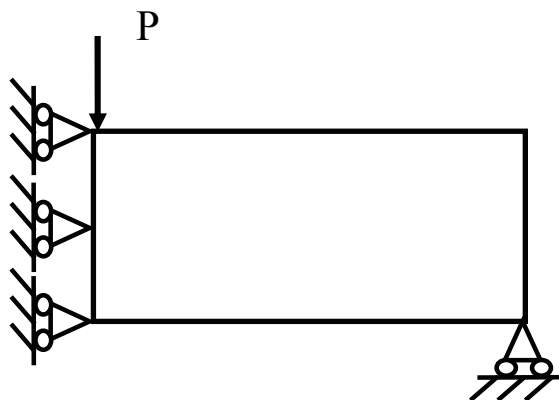


Figure 7: MBB beam (right half-domain)

cellent agreement between the results of meshless method and FEM. However, when FEM does converge to the same topology, the phenomena of mesh-dependency appears (Fig.10(c)) although a filter is applied. The appearance of mesh dependence is a common problem in topology optimization, wherein the solution to the topology optimization changes qualitatively as the mesh is refined. Fortunately, no phenomenon of mesh-dependence is found in the case of MLPG Mixed Collocation Method.

**4.2 Effectiveness of filtering**

Checkerboard patterns are another common problem which are often present in optimal topologies generated by continuum topology optimization methods.

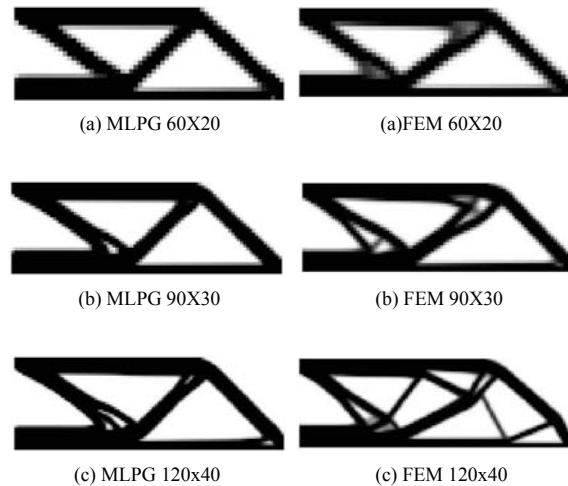


Figure 8: Optimal configuration of MBB beam (halves) by the MLPG Mixed Collocation Method

Figure 9: Optimal configuration of MBB beam (halves) by FEM methods

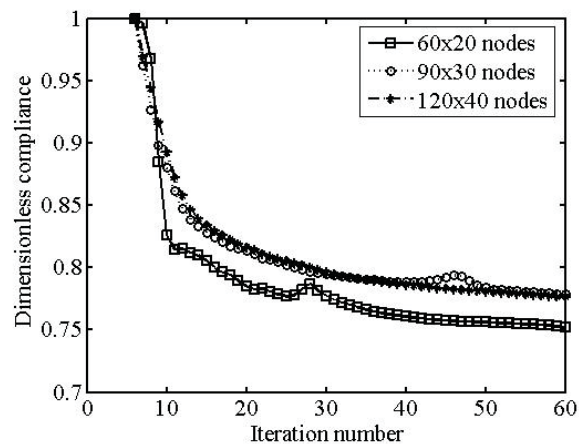


Figure 10: Convergence history of the MBB beam compliance using the present method

Sigmund (1994) suggested a filtering method, which is shown to be effective in suppressing the formation of checkerboard patterns. To illustrate the filtering effect, we consider a cantilever beam in Fig. 11 and a MBB beam in Fig.14.

**Example 3:**

This example is also that of a short cantilever beam which has the rectangular ‘design domain’ (L=2H) as shown in Fig. 11. The load P is applied

at the middle of the right end.

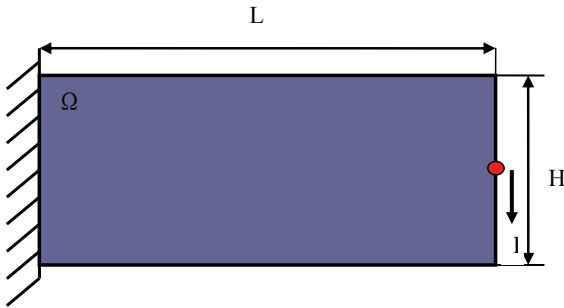


Figure 11: Cantilever beam II ( $L=2H$ )

The design domain is discretized using  $40 \times 20$ ,  $60 \times 30$ ,  $80 \times 40$  uniformly distributed nodes, respectively. For the considered beam, topologies are given in Fig. 12 and Fig.13.

We can see the effects of the filter. A sample MLPG solution with checkerboarding is shown in Fig.12. Fig.13 shows the final optimal layouts of the short cantilever beam after filtering. It can be seen that the checkerboard pattern disappears and optimal configurations became more clear. The filtering properties of the present method are thus verified.

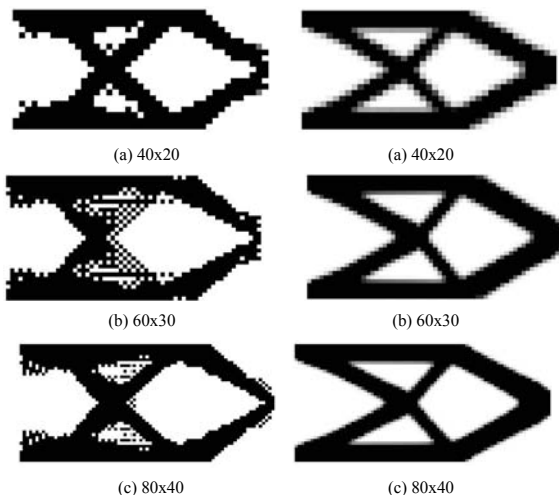


Figure 12: Optimal configuration before filtering

Figure 13: Optimal configuration after filtering

**Example 4:**

We now solve another simple topology optimization problem for various discretization cases, i.e.  $40 \times 20$ ,  $60 \times 30$ ,  $80 \times 40$  uniformly distributed nodes, respectively. The domain and boundary conditions for the problem chosen are shown in Fig. 14. In this case, the beam is of given length  $L$  and depth  $H$ , and both the ends are simply supported. The remaining volume ratio is 30%.

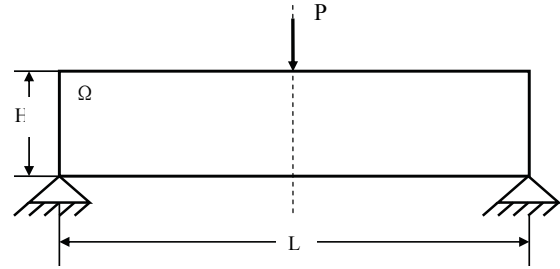


Figure 14: MBB-beam

Fig.15 shows that the algorithm finds a typical bar-design, The results are found to be similar to those in [Eschenauer and Olhoff(2001)]. In this example, we find that the optimum structural layouts are polluted by so-called checkerboard patterns. Figs.16 show that the checkerboards can be completely eliminated by the present nodal sensitivity filter. This example shows that the filter is good for eliminating checkerboarding. As a result of this, it is desirable to suppress the formation of checkerboard patterns in continuum topology optimization.

**4.3 Comparison of topology with different “remaining volume” ratio**

**Example 5:**

The example is that of an MBB beam as in Fig. 17. This case is a bridge-structure with same boundary conditions and different load location as the MBB beam in Example 4. The beam has length  $L$  and depth  $H$  with ratio  $L/H=2$ .

These optimal designs have the “remaining volumes” of 60%, 50%, 40%, 30%, 20% and 10 % of the initial volume, respectively. The final topologies of MBB beam are shown in Fig.18. This design finds a classic Michell type structure and a typical bar-design. The same results can be ob-

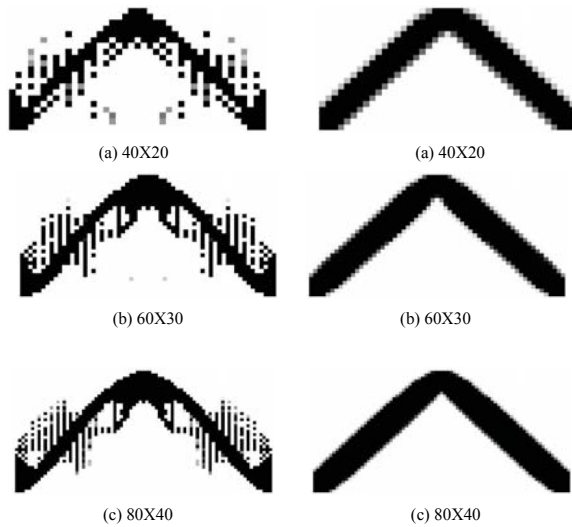


Figure 15: Optimal configuration before filtering

Figure 16: Optimal configuration after filtering

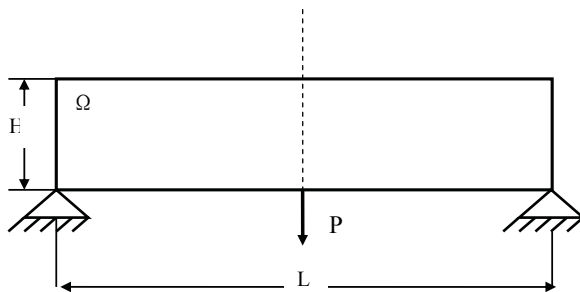


Figure 17: MBB-beam

tained by using Sigmund’s 99 line code in Matlab [Sigmund (2001)].

**Example 6:**

In this example, we consider the initial design of a bridge structure for a prescribed (hatched) area subject to uniformly distributed load (Fig.19). The two points at the bottom surface corners are simply supported. The bridge-structure has a 2:1 ratio for the length:width. The whole structure is modelled by 60×30 nodes. The hatched part is the required minimum thickness at the top of the bridge, which is specified as a non-design domain. We obtain the initial optimal designs for different “remaining volume” limits of 70, 60, 50, 40, 30 and 20 % of the initial volume.

Fig.20 displays an optimal design for the bridge

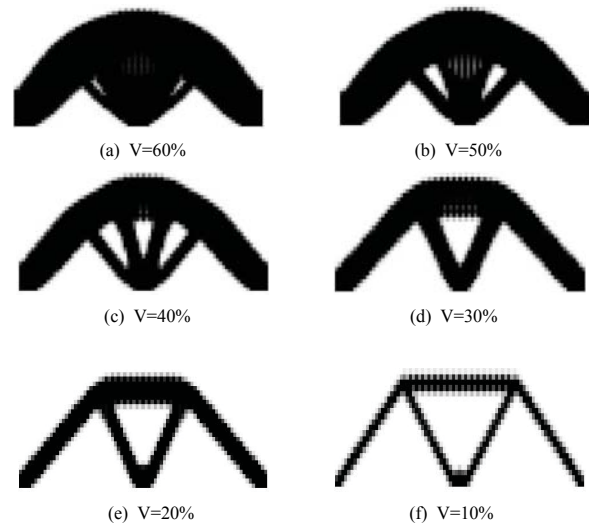


Figure 18: The final topologies of MBB beam with different volume

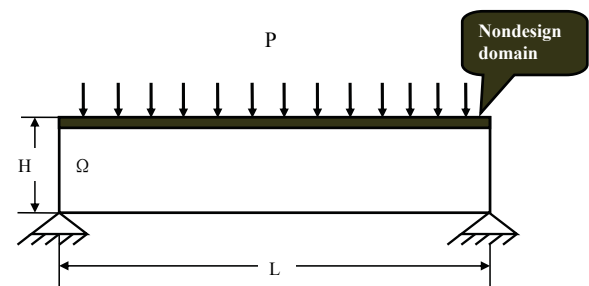


Figure 19: Bridge structure

structure using the conventional MLPG mixed collocation method. When the remaining material volume is less than 50%, the topologically optimized structure is becoming a typical arch truss system. This is a perfect construction that transfers the loads to the supports very efficiently through a reasonable path.

**5 Conclusions**

The MLPG method is implemented to solve the topology optimization problem. In this paper, design domains are discretized by using the MLPG mixed collocation method, and the material distribution problem becomes one of finding the optimal values of the relative nodal volume fractions. A node with zero relative nodal volume fraction represents a void and a node with a relative nodal

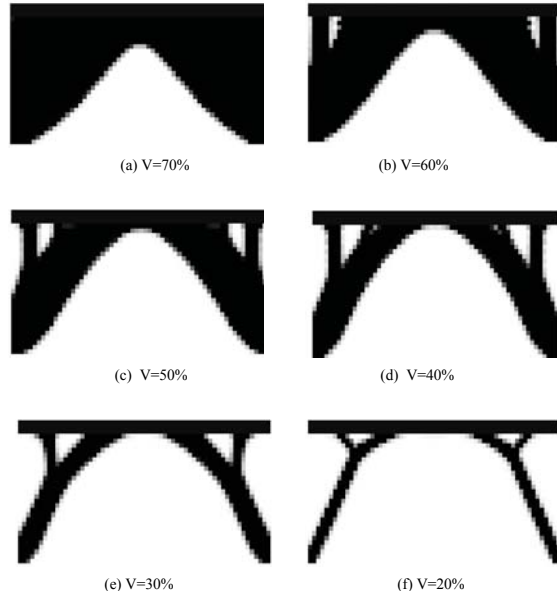


Figure 20: The final topologies of bridge structure with different volume

volume fraction of 1 represents a solid node. The goal is to find a distribution of relative nodal volume fractions that minimizes a compliance objective function, subject to volume constraints. To solve such a topology optimization problem, the popular optimality criteria (OC) method is employed with an iterative heuristic scheme for updating the design variables.

In this paper, we show several numerical examples to demonstrate the validity and convergence of the present method. We examine the effect of filtering on the resulting topology. We compare the various numerical results in solving topology optimization problems. Summarizing our research, the present method has the following advantages:

The filtering technique is not certain in general to suppress the mesh-dependency problem in the finite element method. The present method does not use a mesh of elements. The numerical instability problems related to mesh do not exist. It need not cost extra CPU-time to deal with such the numerical instabilities. The filtering technique is highly suitable for the present MLPG method.

The nodal values are used as the design variables. It can be seen, by comparing with the element-

based methods, that it is not necessary to interpolate or project those design variables onto an element space.

The formulation of the MLPG mixed collocation method is established at the nodal points. It is unnecessary to integrate over the design domain, during the optimization procedure. So the implementation becomes very convenient and efficient.

**Acknowledgement:** This research was conducted during the study of S. Li at UCI. This research was also partially supported by the office of Naval Research.

## References

- Atluri, S.N.; Zhu, T** (1998): A New Meshless Local Petrov-Galerkin (MLPG) Approach in Computational Mechanics, *Computational Mechanics*, Vol.22, pp. 117-127.
- Atluri, S.N., Shen, S.P.** (2002a): The meshless local Petrov-Galerkin (MLPG) method: A simple & less-costly alternative to the finite element and boundary element methods, *CMES: Computer Modeling in Engineering and Sciences*, 3 (1) 11-51.
- Atluri, S.N.; Shen, S.** (2002b): The Meshless Local Petrov-Galerkin (MLPG) Method, 2002, 440 pages, Tech Science Press.
- Atluri, S.N.** (2004) The Meshless Method(MLPG) for Domain & BIE Discretizations, 2004, 680 pages, Tech Science Press.
- Atluri, S.N.; Liu H.T.; Han Z.D.** (2006): Meshless local Petrov-Galerkin (MLPG) mixed collocation method for elasticity problems, *CMES: Computer Modeling in Engineering & Sciences*, vol. 14, no. 3, pp. 141-152.
- Bendsøe, M.P.; Kikuchi, N.** (1988): Generating optimal topologies in optimal design using a homogenization method, *Comp. Meth. Appl. Mech. Engrg*, vol. 71, pp.197–224.
- Bendsøe, M.P.** (1989), Optimal shape design as a material distribution problem, *Struct. Optim.*, vol. 1, pp.193–202.
- Bendsøe, M.P.; Sigmund, O.** (2003): Topology

optimization, theory, methods and applications, Springer.

**Chiandussi, G.; Gaviglio, I.; Ibba, A.** (2004): Topology optimisation of an automotive component without final volume constraint specification, *Advances in Engineering Software* vol. 35, pp.609-617.

**Cisilino, A.P.** (2006): Topology Optimization of 2D Potential Problems Using Boundary Elements, *CMES: Computer Modeling in Engineering & Sciences*, vol.15, no.2, pp.99-106.

**Eschenauer, H.A.; Olhoff, N.** (2001): Topology optimization of continuum structures: A review, *Appl Mech Rev*, vol. 54, no 4, pp.331-390.

**Guest, J.K.; J.H. Prévost, J.K.; Belytschko, T.** (2004): Achieving minimum length scale in topology optimization using nodal design variables and projection functions, *Int. J. Numer. Meth. Engng*; vol. 61, pp.238–254.

**Hansen, L.U.; Horst, P.** (2008): Multilevel optimization in aircraft structural design evaluation, *Computers and Structures*, vol.86, pp.104–118.

**Mackerle, J.** (2003): Topology and shape optimization of structures using FEM and BEM: A bibliography (1999–2001), *Finite Elements in Analysis and Design*, vol. 39, pp. 243–253.

**Norato, J.A.; Bendsøe, M.P.; Haber, R.B.; Tortorelli, D.A.** (2007): A topological derivative method for topology optimization, *Struct Multidisc Optim*, vol. 33, pp. 375–386.

**Sigmund, O.** (1994): Materials with prescribed constitutive parameters: An inverse homogenization problem, *Int. J. Solids Struct.*, vol. 31, pp.2313–2329.

**Sigmund, O.** (1997): On the design of compliant mechanisms using topology optimization, *J. Mech. Struct. Mach.*, vol. 25, pp.493–524.

**Sigmund, O.; Petersson, J.** (1998): Numerical instabilities in topology optimization: a survey on procedures dealing with checkerboards, mesh-dependencies and local minima. *Struct. Optim.*, vol. 16, pp.68–75.

**Sigmund, O.** (2001): A 99 line topology optimization code written in Matlab, *Struct Multidisc Optim.*, vol. 21, pp.120–127.

**Vemaganti, K.; Lawrence, W.E.** (2005): Parallel methods for optimality criteria-based topology optimization, *Comput. Methods Appl. Mech. Engrg.*, Vol.194, pp.3637-3667.

**Wang, S.Y. and Wang, M.Y.** (2006): Structural Shape and Topology Optimization Using an Implicit Free Boundary Parametrization Method, *CMES: Computer Modeling in Engineering & Sciences*, vol.13, no.2, pp.119-147.

**Wang, S.Y.; Lim, K.M.; Khoo, B.C. and Wang, M.Y.** (2007a): A Geometric Deformation Constrained Level Set Method for Structural Shape and Topology Optimization, *CMES: Computer Modeling in Engineering & Sciences*, vol.18, no.3, pp.155-181.

**Wang, S.Y.; Lim, K.M.; Khoo, B.C. and Wang, M.Y.** (2007b): An Unconditionally Time-Stable Level Set Method and Its Application to Shape and Topology Optimization, *CMES: Computer Modeling in Engineering & Sciences*, Vol.21, No.1, pp.1-40.

**Wang, S.Y.; Lim, K.M.; Khoo, B.C. and Wang, M.Y.** (2007c): On Hole Nucleation in Topology Optimization Using the Level Set Methods, *CMES: Computer Modeling in Engineering & Sciences*, vol.21, no.3, pp.219-237.

**Wang, S.Y.; Lim, K.M.; Khoo, B.C. and Wang, M.Y.** (2008): A Hybrid Sensitivity Filtering Method for Topology Optimization, *CMES: Computer Modeling in Engineering & Sciences*, vol.24, no.1, pp.21-50.

**Zhou, M.; Rozvany, G.I.N.** (1991): COC algorithm, Part II: Topological, geometrical and generalized shape optimization, *Computer Methods in Applied Mechanics and Engineering*, vol. 89 ,pp.309-336.

**Zhou, S.; Wang M.Y.** (2006): 3D Multi-Material Structural Topology Optimization with the Generalized Cahn-Hilliard Equations, *CMES: Computer Modeling in Engineering & Sciences*, vol.16, no.2, pp.83-101.